ACS OMEGA

http://pubs.acs.org/journal/acsodf

Article

Efficient Reduction of Cr(VI) with Carbon Quantum Dots

Wei-Min Yang, Fu Liu, Yan-Ting Jin, Zong-Mu Dong, and Guang-Chao Zhao*

Cite This: *ACS Omega* 2022, 7, 23555−23565

Read Online

ACCESS | Metrics & More | Article Recommendations | Supporting Information

ABSTRACT: Hexavalent chromium (Cr(VI)) pollution is a global problem, and the reduction of highly toxic Cr(VI) to less toxic Cr(III) is considered to be an effective method to address Cr(VI) pollution. In this study, low-toxicity carbon quantum dots (CQDs) were used to reduce Cr(VI) in wastewater. The results show that CQDs can directly reduce Cr(VI) at pH 2 and can achieve a reduction efficiency of 94% within 120 min. It is observed that under pH higher than 2, CQDs can activate peroxymonosulfate (PMS) to produce reactive oxygen species (ROS) for the reduction of Cr(VI) and the reduction efficiency can reach 99% within 120 min even under neutral conditions. The investigation of the mechanism shows that the hydroxyl groups on the surface of CQDs can be directly oxidized by Cr(VI) because of the higher redox potential of Cr(VI) at pH 2. As the pH increases, the carbonyl groups on the surface of CQDs can activate PMS to generate ROS, $O_2^{\bullet-}$, and $^1O_2$, which result in Cr(VI) being reduced. To facilitate the practical application of CQDs, the treatment of Cr(VI) in real water samples by CQDs was simulated and the method reduced Cr(VI) from an initial concentration of 5 mg/L to only 8 μg/L in 150 min, which is below the California water quality standard of 10 μg/L. The study provides a new method for the removal of Cr(VI) from wastewater and a theoretical basis for practical application.

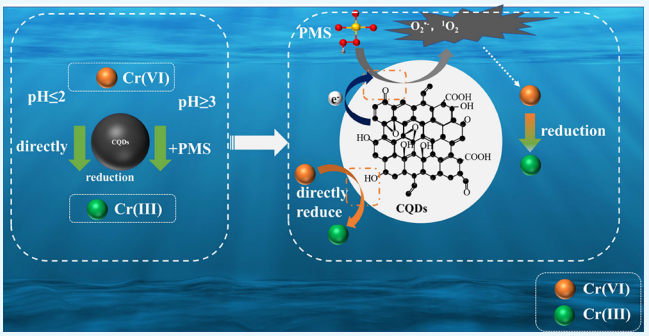

1. INTRODUCTION

Chromium exists in two primary forms in aqueous environments: trivalent and hexavalent.[1,2] Cr(III) is an all-important additive for animal growth and metabolism.[3,4] In contrast, Cr(VI) is carcinogenic, teratogenic, and mutagenic to animals and human beings, and the high mobility of Cr(VI) also poses an assertive threat to the environment.[5,6] As a result, highly hazardous Cr(VI) must be removed from wastewater.

In adjustment to abate the toxicity of Cr(VI) in wastewater, a growing array of treatments has been developed, including reduction,[7−9] adsorption,[10] and membrane separation.[11] Compared with these technologies, the advanced oxidation process (AOP) has attracted more and more attention due to its simple operation, high efficiency, low energy consumption, and ability to treat multiple pollutants.[12−14] Peroxymonosulfate (PMS)-based AOPs produce various ROS such as hydroxyl radicals (•OH), sulfate radicals ($SO_4^{\bullet-}$), and superoxide radicals ($O_2^{\bullet-}$), which can effectively reduce Cr(VI) to Cr(III). PMS can be activated by different means such as ultrasound, UV, metal catalysis, and carbonaceous materials.[15−18] Compared to other activation methods, carbon-based catalysts are receiving much attention from researchers due to the large number of functional groups on the surface that can produce efficient catalytic properties.[19]

Carbon quantum dots (CQDs) are carbon nanomaterials with sizes below 10 nm.[20] CQDs have plentiful, inexpensive, one-of-a-kind electron transfer capabilities and a large specific surface area, granting them with excellent chemical property performance.[21] The large number of functional groups on the surface of CQDs can be both oxidized and activated by PMS. However, there are still a few reports on the advanced oxidation technology of CQDs. Therefore, we looked into not only the direct reduction of Cr(VI) by CQDs but also how CQDs activate PMS to produce reactive oxygen species for Cr(VI) reduction.

In this research, CQDs are acclimated not only as reducing agents but also as activators. Furthermore, Cr(VI) was chosen as the target contaminant to estimate the reduction and catalytic capacity of CQDs. The conclusions show that C═O on the surface of CQDs plays an acute role in the activation of PMS for the reduction of Cr(VI), according to functional group shielding tests and XPS energy spectroscopic analysis. As a result, CQDs can reduce Cr(VI) directly at lower pH while also activating PMS to create ROS for Cr(VI) reduction at higher and wider pH ranges.

Received: April 5, 2022
Accepted: June 17, 2022
Published: June 29, 2022

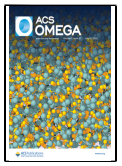

https://doi.org/10.1021/acsomega.2c02063
ACS Omega 2022, 7, 23555−23565

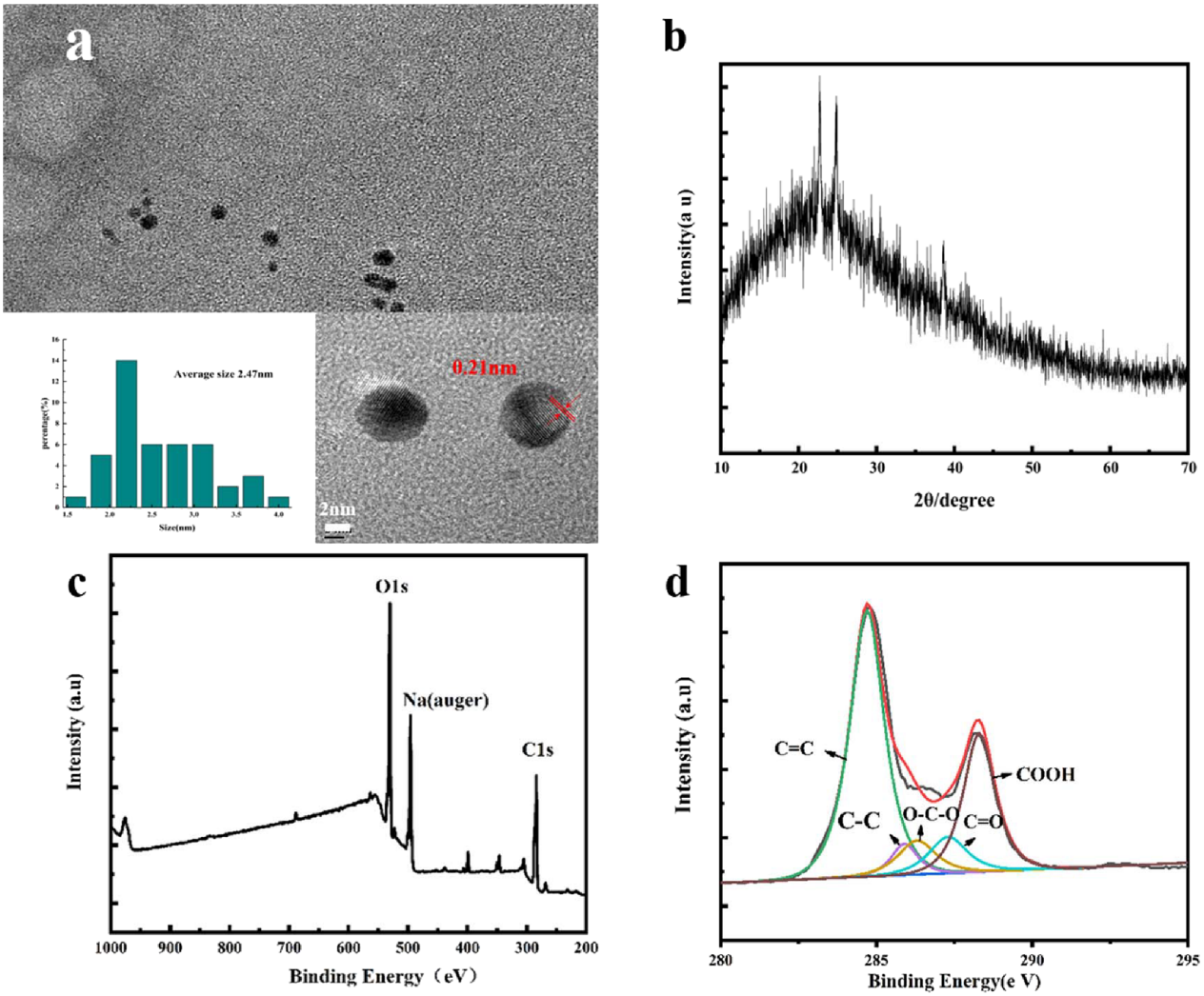

Figure 1. (a) Size distribution of particles, HRTEM image (inset), and TEM image, (b) XRD pattern, (c) survey XPS spectrum, and (d) high-resolution C1s spectra of the as-prepared CQDs.

2. MATERIALS AND METHODS

2.1. Chemicals. All reagents were of analytical purity and were not further purified. The water used for the experiments was deionized water (18.25 MΩ·cm).

2.2. Instrumentations. The morphology of the sample was observed by TEM (FEI Talos F200X, US). Surface compositions of the sample were obtained by XPS (Axis Ultra DLD Kratos AXIS SUPRA, Japan). A Nexus 670 was used to observe the Fourier transform infrared (FT-IR) spectra (US). An Ultima IV diffractometer was used to record CQD X-ray diffraction (XRD) curves (Japan). The maximum absorption wavelength of the material was recorded by a UV−vis spectrophotometer (300/PE Lambda 750S, US). The fluorescence spectra were obtained by an F98 fluorescence spectrophotometer (China).

2.3. Preparation of CQDs. CQDs were prepared by a one-step hydrothermal method,[22] applying both ammonium bicarbonate and sodium citrate reagents under high temperature and loading conditions. The synthesis of CQDs required 0.4 g of sodium citrate and 3.0 g of ammonium bicarbonate to be dissolved in 60 mL of ultrapure water, and then these mixtures were transferred to the reaction kettle and put into the oven for 7 h at 180 °C. Further purification of CQDs in water by a dialysis bag for 24 h was carried out. The dialyzed solution was evaporated to dryness in an evaporating dish to obtain CQDs, and the as-prepared CQDs were stored in a refrigerator at 4 °C.

3. RESULTS AND DISCUSSION

3.1. Characterization of CQDs. The as-prepared CQDs, synthesized according to ref 22, were characterized as follows. TEM imaging (as shown Figure 1a) clearly reveals the uniform distribution of CQDs. The particle size of CQDs ranges from 1.5 to 5.5 nm, with an average particle size of 2.47 nm. The interplanar spacing of 0.21 nm lattice stripes can be detected by HRTEM (Figure 1a), similar to the previous study.[23] The XRD pattern of CQDs (Figure 1b) shows a broad peak at 22° (0.33 nm), which is mainly the effect of carbon atoms.[24] Several different surface functional groups such as C═C, C−C, C−O−C, and C═O were observed by XPS (Figure 1c), and these functional groups were also observed on FT-IR (Figure S1). As shown in Figure S2a, a UV−vis absorption peak at 365 nm was observed.[22] The PL spectra (Figure S2b) revealed the strongest emission peak at 445 nm, which was followed by the excitation peak at 350 nm.[25] According to the above characterization results, the morphological properties of CQDs are similar to those of previous studies, indicating that CQDs were auspiciously prepared. The shape of the nitrogen adsorption and desorption curves of the CQDs allows them to be classified

https://doi.org/10.1021/acsomega.2c02063
ACS Omega 2022, 7, 23555−23565

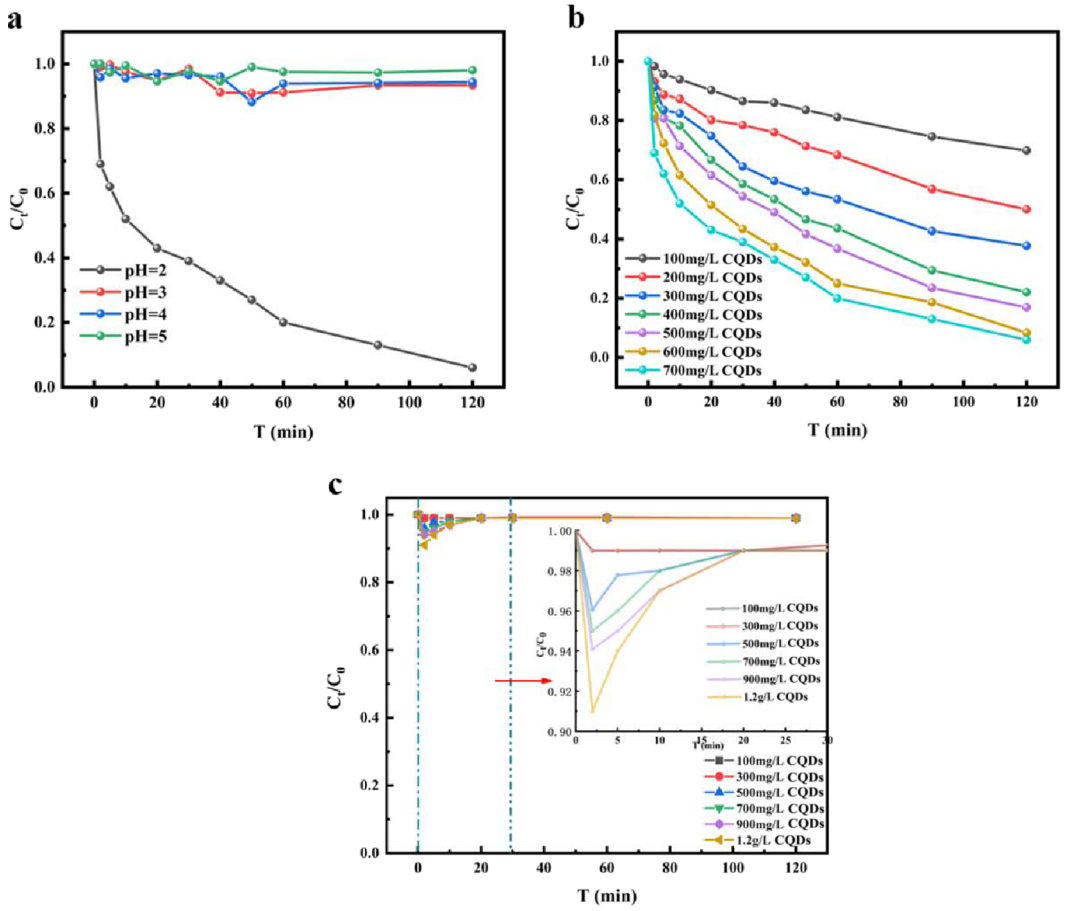

Figure 2. (a) Direct reduction of Cr(VI) by CQDs under different pH conditions, (b) direct reduction of Cr(VI) by different concentrations of CQDs at pH 2, and (c) direct reduction of Cr(VI) with different concentrations of CQDs at pH 7.

as type III with H3 loops according to the IUPAC classification, with a BET specific surface area of 9.284 m^2/g and an average pore size of 1.27 nm (Figure S3). Similarly, the isoelectric point on the surface of CQDs was further explored and, from Figure S4, it can be seen that the zeta potential decreases with increasing pH, indicating that CQD suspended particulate matter is more stable with increasing pH.

3.2. Direct Reduction of Cr(VI) with CQDs. Cr(VI) exists in water in different anionic forms, including $HCrO_4^-$, $Cr_2O_7^{2-}$, and CrO_4^{2-}. As the pH of the solution changes, these Cr(VI) anionic forms can be converted to each other.[26] In the solution, $Cr_2O_7^{2-}$ and CrO_4^{2-} are in dynamic equilibrium, and when the solution is acidic, the reaction shifts to the left (eq 1) and $Cr_2O_7^{2-}$ is spontaneously converted to $HCrO_4^-$ as the primary substance (eq 2). Cr(VI) is considered to be a very strong oxidant due to its high redox potential (eq 3). Similarly, when the pH in the solution rises, the equilibrium shifts to the right (eq 1) and, finally, CrO_4^{2-} is the only chromate in the solution.[27] It can be apparent that when the solution pH is different, the ionic form of Cr(VI) will also be altered and its redox potential will also be different. pH has an absolute result on the redox potential of Cr(VI).

$$Cr_2O_7^{2-} + H_2O \leftrightarrow 2CrO_4^{2-} + 2H^+ \quad (1)$$

$$Cr_2O_7^{2-} + H^+ \rightarrow 2HCrO_4^- + 2H_2O \quad (2)$$

$$HCrO_4^- + 7H^+ + 3e^- \rightarrow Cr(III) + 4H_2O,\ E^\circ = 1.33\ V \quad (3)$$

The surface of the produced CQDs comprises a high number of functional groups, which may have reduced capabilities. Therefore, Cr(VI) reduced directly with CQDs was first investigated. The findings of direct reduction of Cr(VI) by CQDs at various initial pH values are shown in Figure 2a. When the pH is 2, Cr(VI) can be directly reduced with CQDs, in which the reduction efficiency can reach 94% at 120 min. However, when the pH is equal to or over 3, Cr(VI) can hardly be reduced. According to a previous study,[28] Cr(VI) shows a very high positive redox potential (about +1.33 V) at pH 2, which means that Cr(VI) is a strong oxidant and can be reduced in the presence of electron donors. Correspondingly, the CQD surface has an ample number of electron-rich functional groups, such as carboxyl, hydroxyl, and carbonyl groups, which can be oxidized at pH 2.[29] Furthermore, as can be seen in Figure 2b, the reduction efficiency of Cr(VI) improves as the concentration of CQDs increases. When the amount of CQDs was increased to 700 mg/L, 94% of Cr(VI) could be reduced after 120 min. However, because the redox potential of Cr(VI) rapidly decreases with increasing pH, Cr(VI) cannot be reduced by CQDs at pH 7, even under a higher concentration of CQDs (as shown in Figure 2c). As can be seen from the enlarged graph (inset), there was a certain decrease in Cr(VI) in the system from 0 to 2 min as the amount of CQDs increased. Due to this process, Cr(VI) was adsorbed by CQDs and then Cr(VI) was quickly desorbed from the water again and returned to its initial concentration, indicating that the adsorption of Cr(VI) by CQDs was not significant.

https://doi.org/10.1021/acsomega.2c02063
ACS Omega 2022, 7, 23555−23565

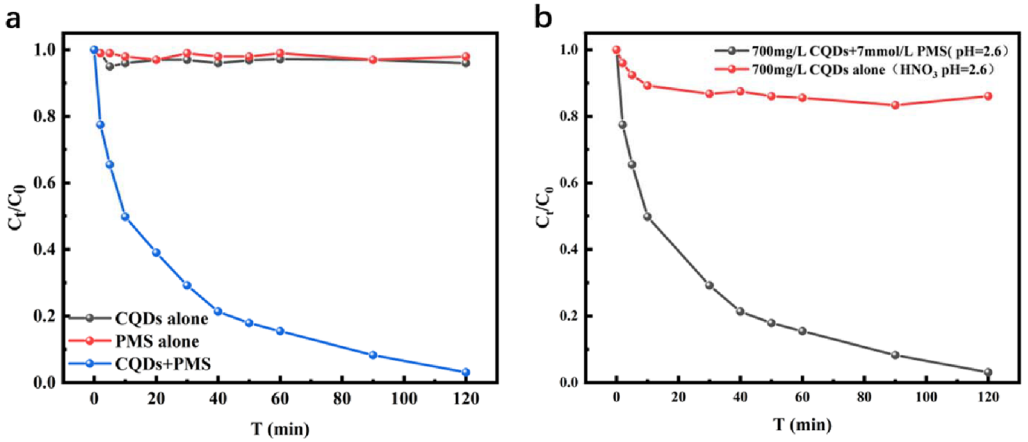

Figure 3. (a) Reduction of Cr(VI) by CQDs alone, PMS alone, and CQDs/PMS at pH 7. (b) Reduction of Cr(VI) at pH 2.6 by 700 mg/L CQDs alone and by 700 mg/L CQDs and 7 mmol/L PMS together.

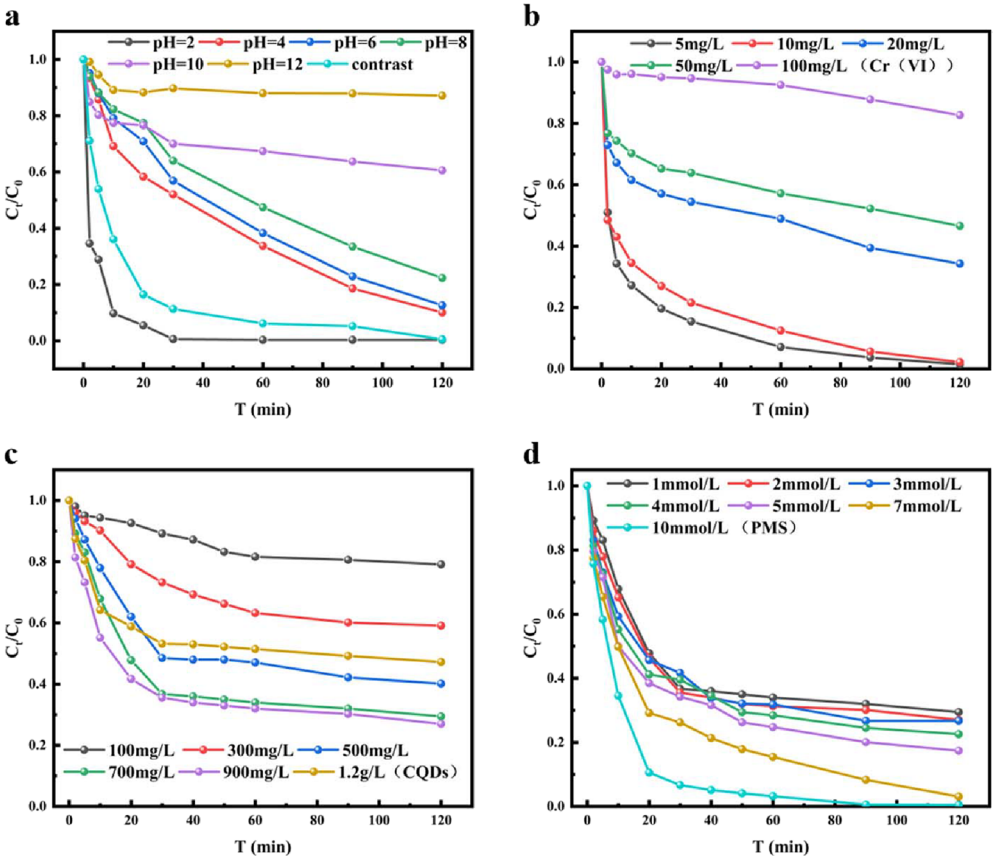

Figure 4. (a) Effect of different initial pH values on the Cr(VI) reduction in the CQDs/PMS system. (b) Cr(VI) reduction under the conditions of different initial Cr(VI) concentrations. (c) Effect of the loading of CQDs on the Cr(VI) reduction in the PMS/CQDs system ([PMS] =1 mmol/L). (d) Effect of the loading of PMS on the Cr(VI) reduction in the CQDs/PMS system.

However, the efficiency of the direct Cr(VI) reduction by CQDs is relatively low and the pH requirement is strict (equal to or less than 2). Therefore, PMS was introduced into this system, expecting that CQDs can activate PMS to generate ROS for Cr(VI) reduction, thus improving the reduction efficiency in a wider pH range.

3.3. Reduction of Cr(VI) by the CQDs/PMS Systems.

3.3.1. Reduction Efficiency of Cr(VI) by the CQDs/PMS System. A control experiment was undertaken to assess the CQDs/PMS system's reduction efficiency. Figure 3a reveals the results of Cr(VI) reduction under different conditions. When 700 mg/L CQDs or 7 mmol/L PMS was added separately to the pH-neutral Cr(VI) solution, it can be observed that the concentration of Cr(VI) in the solution remained essentially unchanged within 120 min. However, when CQDs and PMS are added into the reaction system at the same time, Cr(VI) can be rapidly reduced, about 99% within 120 min. There are two accessible reasons for this phenomenon. The first possibility is that the addition of PMS acidifies the solution, which causes an increase in the oxidation of Cr(VI), leading to Cr(VI) oxidizing the hydroxyl functional group on the basis of CQDs. Another

https://doi.org/10.1021/acsomega.2c02063
ACS Omega 2022, 7, 23555−23565

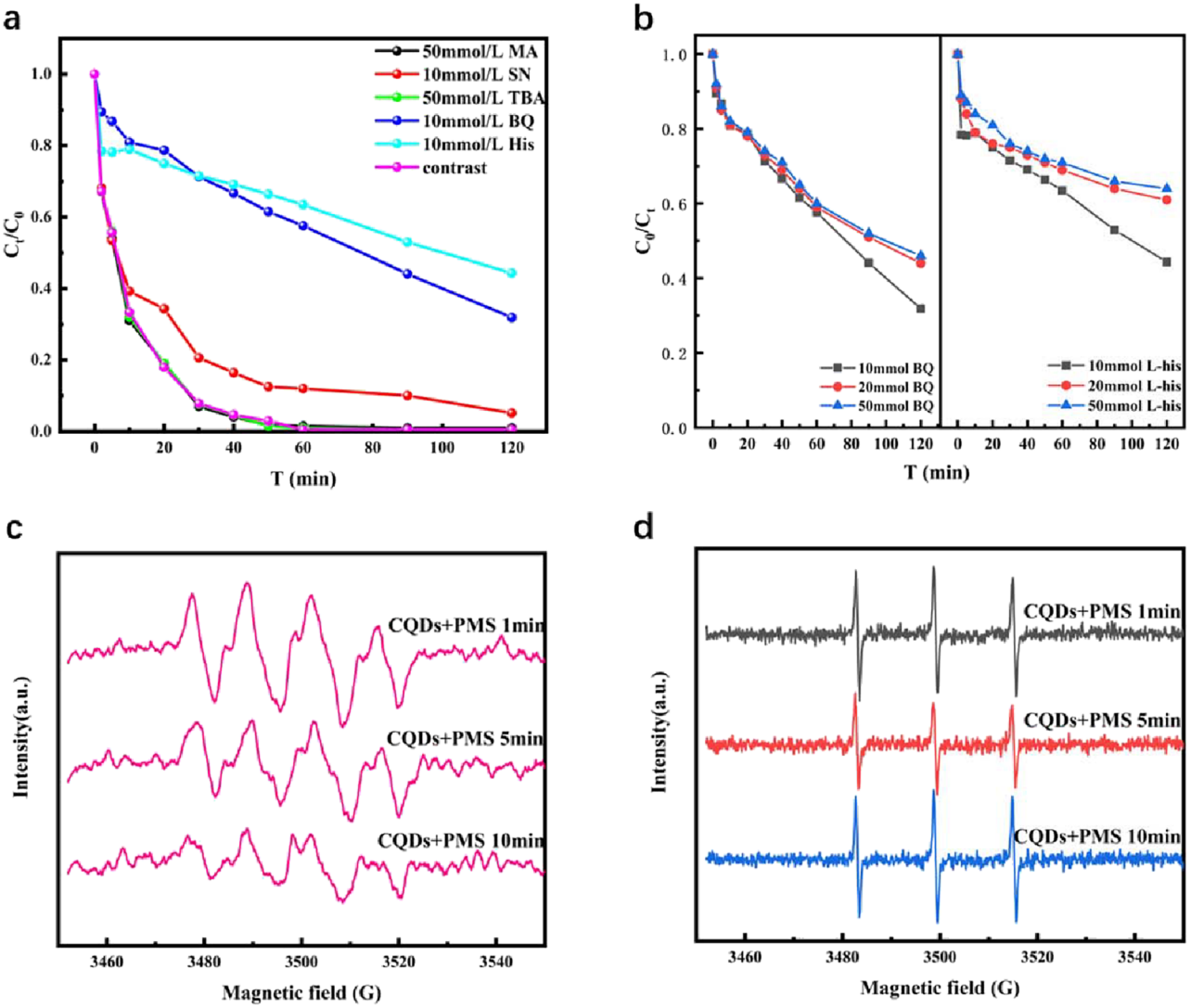

Figure 5. (a) Effects of various quenching agents and (b) different concentrations of BQ and L-His on Cr(VI) reduction. EPR spectra obtained from the CQDs/PMS system in the presence of (c) DMPO and (d) TEMP.

possibility is that some substances are produced by CQDs and PMS, causing the reduction of Cr(VI).

To verify whether PMS merely adjusted the pH of the solution to cause a strongly acidic solution, a comparative experiment was performed. When PMS was added to the solution up to 7 mmol/L, the pH of the solution was about 2.6. Then, the solution was adjusted to the same pH (2.6) with 5% HNO_3, in which direct reduction of Cr(VI) by CQDs was performed. As shown in Figure 3b, only 14% of Cr(VI) can be directly reduced by CQDs within 120 min under this pH condition, suggesting that the reduction of most Cr(VI) in solution may be due to some substances produced by PMS and CQDs. The substances should be the ROS produced through CQDs activating PMS.

3.3.2. Effect of Different Conditions on the Reduction of Cr(VI) by the CQDs/PMS System. It is well accepted that pH is a critical factor in the treatment of Cr(VI) wastewater.[30] This is because the pH profoundly affects the redox potential of Cr(VI). Redox of Cr(VI) and solution acidity are positively correlated (E° = 1.33 V).[31] As shown in Figure 4a, the reduction efficiency values of Cr(VI) by CQDs/PMS are about 99, 90, 87, and 78% at pH 2, 4, 6, and 8, respectively. Even under strongly alkaline pH conditions (pH = 10), still 40% of Cr(VI) can be reduced by CQDs/PMS within 120 min. However, 99% of Cr(VI) was reduced within 50 min when the pH was 2. At this pH, Cr(VI) can not only oxidize directly the hydroxyl groups on the surface of CQDs but also can be reduced with the ROS produced by CQDs/PMS, resulting in a greatly increased reduction efficiency. According to the previous discussion, when the pH is more than 2, the direct reduction of Cr(VI) in solution by CQDs becomes difficult. So, the reduction of Cr(VI) at higher pH is mainly due to the ROS from the CQDs/PMS system. The high reduction efficiency of Cr(VI) still can be obtained at a wide pH range, even up to pH 8, demonstrating the good pH adaptability of the CQDs/PMS system.

Different concentrations of Cr(VI) were used to probe the stability of CQDs/PMS. When the Cr(VI) concentration was increased from 5, 10, 20, and 50 to 100 mg/L, the reduction efficiency of Cr(VI) decreased from 99, 98, 65, and 53 to 17% (as shown in Figure 4b), respectively, within 120 min. In fact, the concentration of CQDs and PMS affects the amount of ROS in the solution. On the one hand, the fewer CQDs can only provide a limited number of accessible active sites for the activation of PMS, only producing a fixed amount of ROS for reduction of

https://doi.org/10.1021/acsomega.2c02063
ACS Omega 2022, 7, 23555−23565

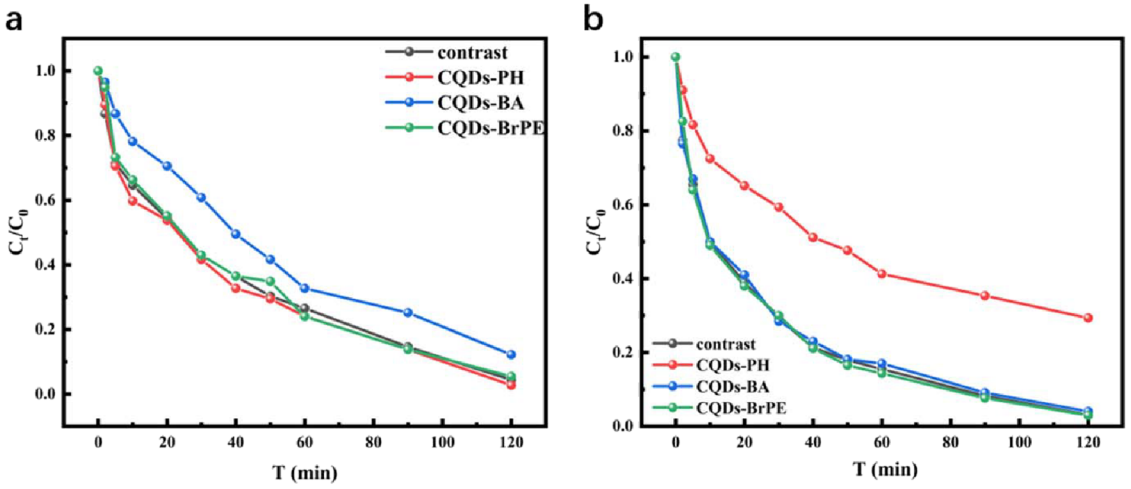

Figure 6. (a) Performance of CQDs and CQD derivatives for the direct reduction of Cr(VI) at pH 2. (b) Effects of CQDs and CQD derivatives on the Cr(VI) reduction in the presence of PMS.

Cr(VI).[32] Meanwhile, the limited amount of PMS cannot produce enough ROS to reduce Cr(VI). Under this condition, by properly increasing the amount of CQDs and PMS, the high initial concentration of Cr(VI) can also be fully reduced within 120 min. On the other hand, under a lower amount of CQDs and PMS, the insufficient rate of ROS production may also affect the reduction rate of Cr(VI), which makes high initial concentrations of Cr(VI) not be sufficiently reduced within 120 min. Under this condition, fully prolonging the reaction time can also obtain a satisfactory reduction efficiency, as shown in Figure S5. Cr(VI) can be fully reduced after 13 h for 20 and 50 mg/L initial concentrations of Cr(VI), and even for the 100 mg/L initial concentration of Cr(VI), 90% of Cr(VI) can also be reduced after 24 h. However, the concentration of Cr(VI) in actual wastewater samples is generally much lower. So, in this investigation, the initial concentration of Cr(VI) was set at 5 mg/L.

To investigate the effect of CQD dosage on the reduction of Cr(VI), a batch of experiments was performed with different CQD dosage from 0.1 to 1.2 g/L. As observed in Figure 4c, with increasing concentration of CQDs from 100 to 700 mg/L, the reduction efficiency of Cr(VI) was gradually boosted when the initial concentration of Cr(VI) was 5 mg/L. But the efficiency tends to be stable when the concentration of CQDs increases from 700 to 900 mg/L. On the one hand, increasing the loading of CQDs will accelerate the reduction of Cr(VI) by providing more active sites for the activation of PMS. On the other hand, further increasing the amount of CQDs, the increase in the reduction efficiency of Cr(VI) is not obvious because the concentration of Cr(VI) determines the entire redox reaction under this condition. Considering that the reduction of Cr(VI) was comparable within 120 min, 700 mg/L CQDs were chosen to continue the following experiments.

The effect of PMS concentrations on Cr(VI) reduction was also further studied. As shown in Figure 4d, with the increase in PMS concentration, the amount of Cr(VI) reduction in the system was enhanced. This is due to the fact that increasing the concentration of PMS not only increases the ROS production but also makes the solution more acidic, leading to a higher redox potential of Cr(VI). When the concentration of PMS is more than 7 mmol/L, Cr(VI) in solution is almost reduced within 120 min. So, 7 mmol/L PMS was chosen to continue the following experiments.

4. MECHANISM OF CR(VI) REDUCTION BY PMS ACTIVATION WITH CQDS

The above experiments show that Cr(VI) is reduced by the activation of PMS with CQDs to produce ROS. To determine the Cr(VI) reduction mechanism in the CQDs/PMS system, a series of radical scavengers were therefore introduced into the system. $SO_4^{\bullet-}$ (3.2×10^6 M^{-1} s^{-1}) and •OH (9.7×10^8 M^{-1} s^{-1}) can be removed by methanol (MA), whereas *tert*-butanol (TBA) is a specific scavenger for •OH (3.8×10^8 to 7.6×10^8 M^{-1} s^{-1}).[33] $O_2^{\bullet-}$ (0.9×10^9 to 1×10^9 M^{-1} s^{-1}) can be selectively scavenged by *p*-benzoquinone (BQ).[34] $AgNO_3$ (SN) is used as an electron (e^-) eliminator,[35] while L-histidine (His) is a scavenger of $^1O_2$ (1×10^9 M^{-1} s^{-1}).[36] The effects of the above scavengers on Cr(VI) reduction are shown in Figure 5a. The results indicate that the inhibition of Cr(VI) reduction by TBA and MA was negligible, indicating that neither •OH nor $SO_4^{\bullet-}$ is the main ROS. On the contrary, the presence of *p*-benzoquinone significantly decreases the reduction of Cr(VI) from 99 to 68%, indicating that $O_2^{\bullet-}$ may play a major role in the Cr(VI) reduction. In addition, the addition of SN slightly decreases the Cr(VI) reduction efficiency from 99 to 95%, indicating that the activation efficiency of CQDs/PMS is decreased by the addition of SN. However, the addition of SN slightly inhibited the reduction of Cr(VI) by CQDs/PMS, suggesting a possible electron transfer between CQDs and PMS.[35] Simultaneously, the addition of His contributed to a dramatic decrease of Cr(VI) from 99 to 55%, implying that $^1O_2$ may play an additional essential role in Cr(VI) reduction. Similarly, different concentrations of BQ and L-His were added individually to the CQDs/PMS system, and it can be seen from Figure 5b that the reduction of Cr(VI) was not significantly inhibited when excess BQ and L-His were added, indicating that the reduction of Cr(VI) was not a reactive oxygen species in action, whereas when BQ and L-His were added together to CQDs/PMS (Figure S6), Cr(VI) was essentially not reduced. Therefore, the results of the quenching experiments showed that $O_2^{\bullet-}$ and $^1O_2$ may be two major ROS species during the activation reactions of PMS by CQDs.

In addition, the ROS produced by the CQDs/PMS system were further characterized by EPR tests. As shown in Figure 5c, four characteristic peaks of the EPR signal were observed, representing the DMPO-$O_2^{\bullet-}$ adduct, which displays the

https://doi.org/10.1021/acsomega.2c02063
ACS Omega 2022, 7, 23555−23565

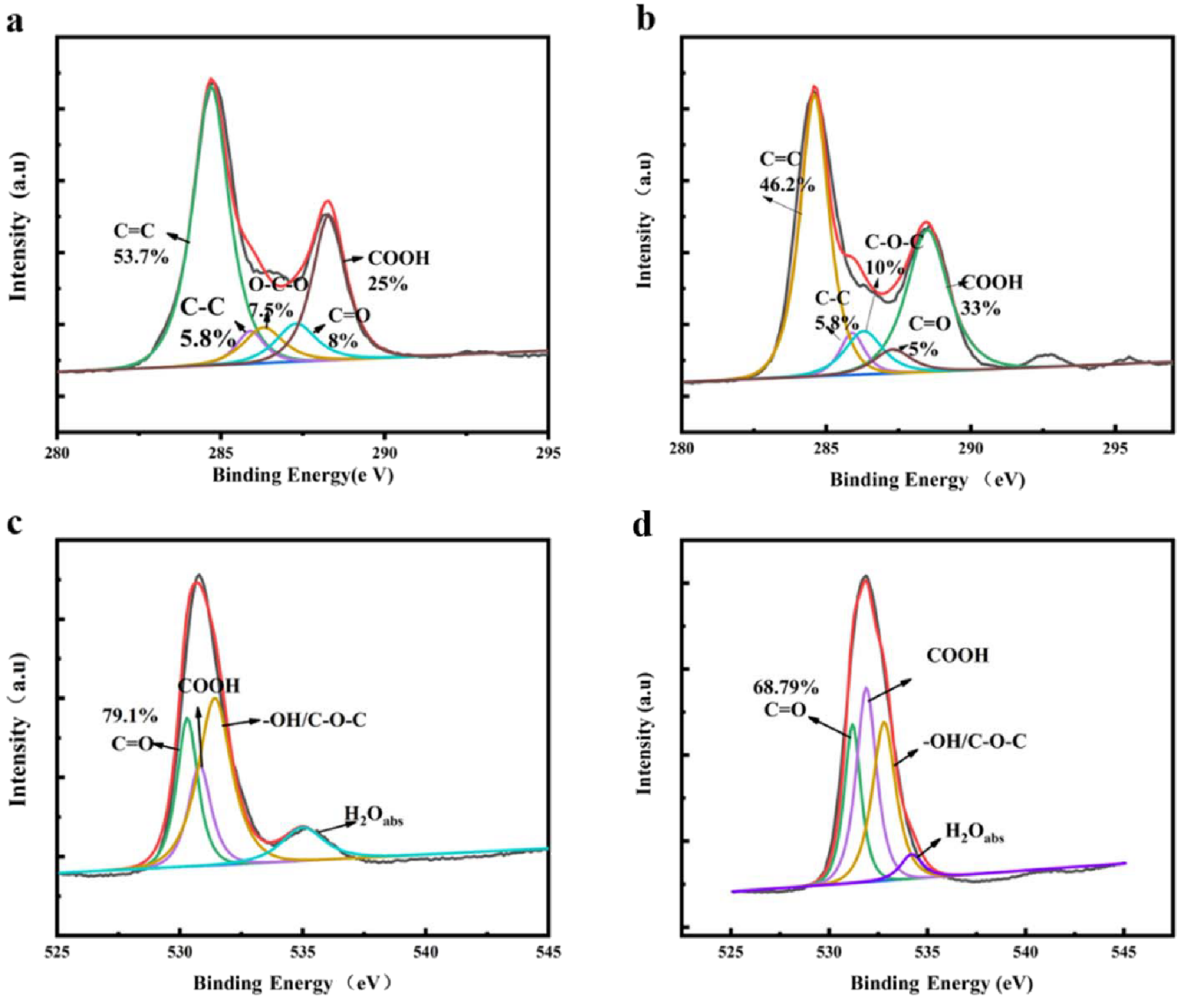

Figure 7. High-resolution C1s XPS spectra of CQDs (a) before reaction and (b) after reaction and high-resolution O1s XPS spectra of CQDs (c) before reaction and (d) after reaction.

generation of $O_2^{\bullet-}$ radicals. In addition, Figure 5b also clearly shows that the production of $O_2^{\bullet-}$ radicals is constantly decreasing with reaction time. On the other hand, as shown in Figure 5d, the typical 1:1:1 triplet signal representing $^1O_2$ is also obtained by using TEMP as the spin trapper of the EPR test.[37] Moreover, its signal intensity remained constant throughout the reaction time. The obtained EPR spectra of $O_2^{\bullet-}$ and $^1O_2$ (Figure 5c,d) are consistent with those reported in a previous study.[38] The EPR results further suggest that $O_2^{\bullet-}$ and $^1O_2$ are the two major reactive oxygen species in the reaction system, which is also consistent with the radical quenching experiments. In addition, as can be seen from Figure 5c, it also clearly explains why the rapid decrease in Cr(VI) concentration at the beginning of the reaction subsequently slows down, which is due to the fact that the production of $O_2^{\bullet-}$ decreases over time.

Surface functional groups of carbon materials such as −COOH, −OH, and C═O are very essential electron donors.[39] Similarly, CQDs contain considerable amounts of carbonyl, hydroxyl, and carboxyl groups at their basal planes and surfaces.[40] Therefore, it is necessary to clarify which group plays the main role in the activation of PMS and the direct reduction of Cr(VI). In this study, these functional groups on the interface of CQDs were shielded respectively to demonstrate the role of these functional groups in the direct reduction of Cr(VI) and the activation of PMS. The process of generating CQD derivatives is shown in Figure S1 and Scheme S1. Similarly, FT-IR showed a corresponding decrease in these functional groups (Figure S7).

The direct reduction of Cr(VI) by CQDs and CQD derivatives at pH 2 is shown in Figure 6a. Compared to the untreated CQDs, the derivative CQDs-BA (shielding hydroxyl) showed a slight inhibition for the direct reduction of Cr(VI) from 94 to 84% after 120 min under the aforementioned conditions, while the other two derivatives, CQDs-PH (shielding carboxyl) and CQDs-BrPE (shielding carbonyl), show essentially no inhibition, suggesting that −OH on the surface of CQDs may be the main reducing group, enabling the direct reduction of Cr(VI) at pH 2. This result is similar to previous studies stating that Cr(VI) can oxidize −OH on the surface of carbon materials under strongly acidic conditions (eq 4).[41,42]

$$-C-OH + HCrO_4^- + 6H^+ \rightarrow -C{=}O + 2Cr^{3+} + 4H_2O \quad (4)$$

It was also investigated that functional groups are involved in the activation of PMS. As illustrated in Figure S8, individual CQDs or CQD derivatives cannot directly reduce Cr(VI) under the condition of neutral pH. However, in the presence of PMS, CQDs and all CQD derivatives can cause Cr(VI) to be reduced.

https://doi.org/10.1021/acsomega.2c02063
ACS Omega 2022, 7, 23555−23565

Scheme 1. Proposed Mechanism for Cr(VI) Reduction via CQD and CQDs/PMS Processes

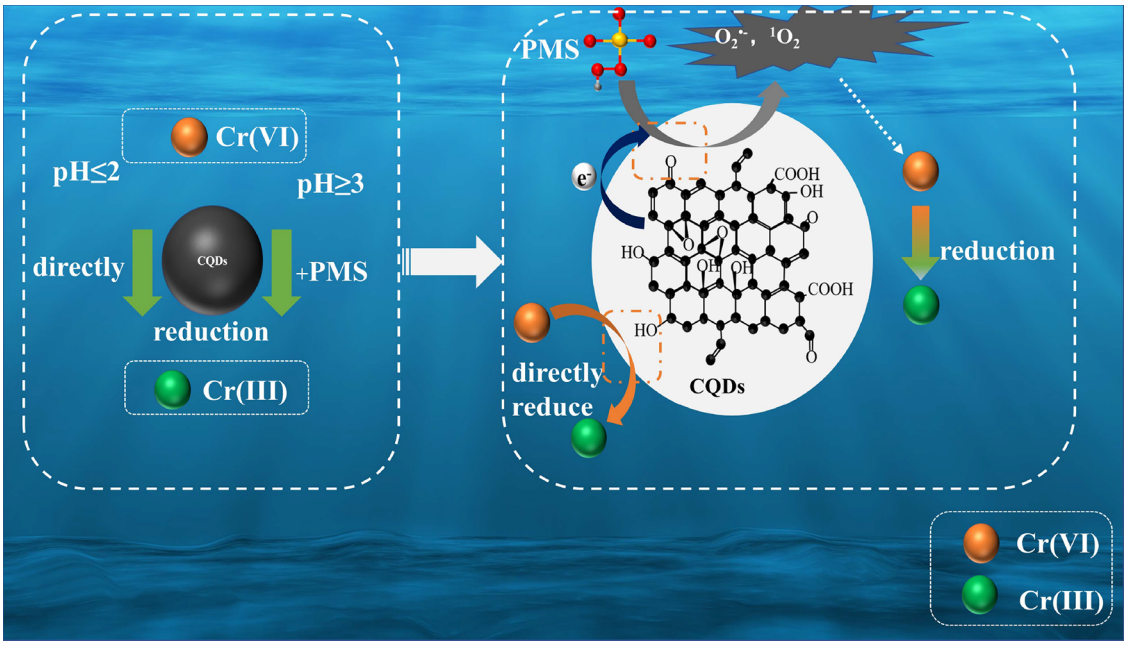

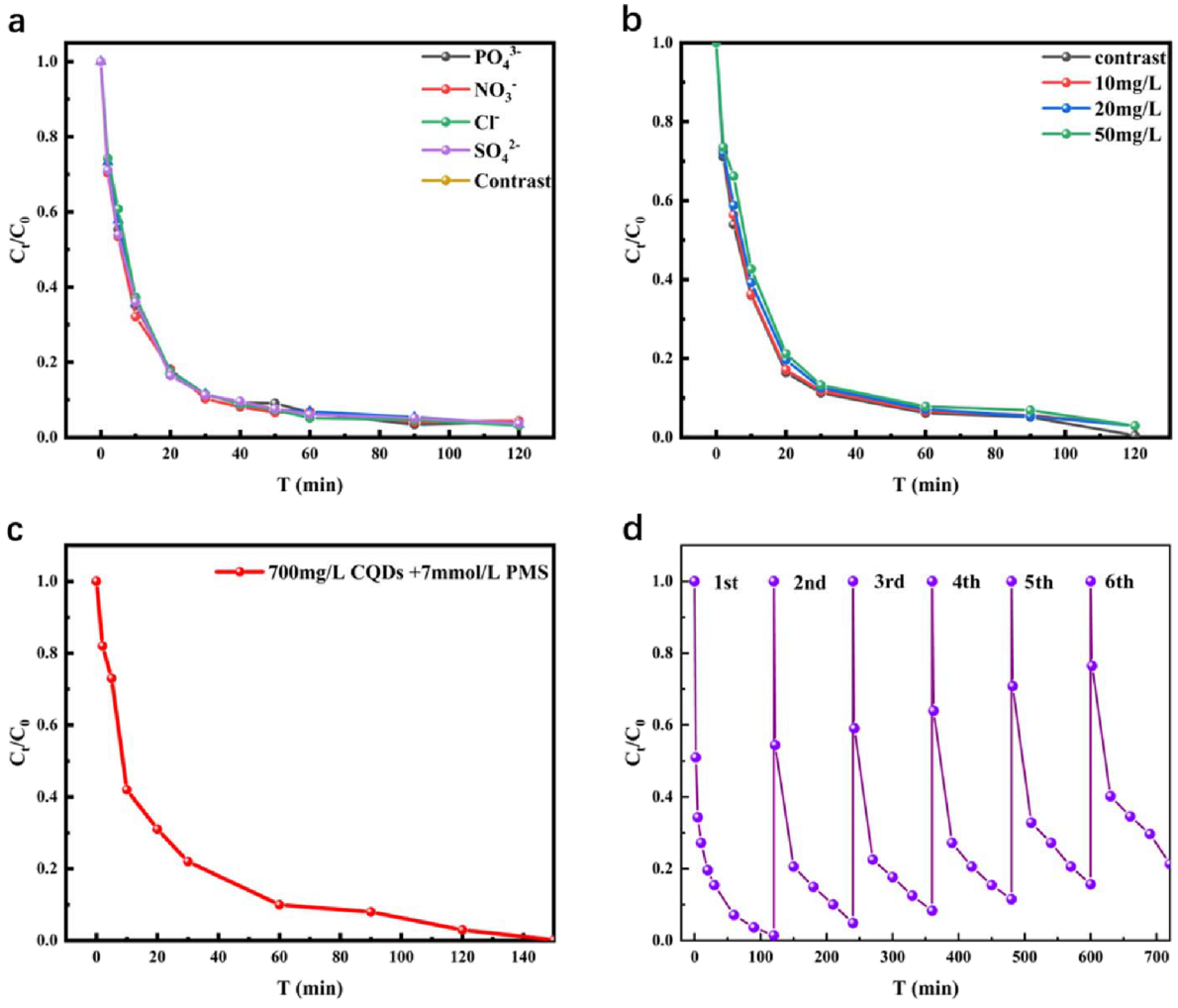

Figure 8. (a) Effect of coexisting anions on Cr(VI) reduction by CQDs/PMS, (b) effect of HA on the reduction of Cr(VI) by CQDs/PMS, (c) reduction of Cr(VI) in the simulated wastewater sample by CQDs/PMS, and (d) cyclic experiments of CQDs/PMS for Cr(VI) reduction ([Cr(VI)]: 5 mg/L; [PO_4^{3-}]: 50 mg/L; [NO_3^-]: 50 mg/L; [Cl^-]: 50 mg/L; [SO_4^-]: 50 mg/L; pH = 7).

https://doi.org/10.1021/acsomega.2c02063
ACS Omega 2022, 7, 23555−23565

Compared with CQDs/PMS, the efficiency of Cr(VI) reduction by CQDs-BA/PMS and CQDs-BrPE/PMS is almost unchanged, suggesting that the hydroxyl group (−OH) and carboxyl group (−COOH) may not play a decisive role in the reduction of Cr(VI). However, the Cr(VI) reduction efficiency obviously decreases from 99 to 78% in the CQDs-PH/PMS system, indicating that the carbonyl group (C═O) may have an important role in activating PMS to generate $O_2^{\bullet-}$ and $^1O_2$. In other words, there are no effects on the reduction of Cr(VI) after shielding the COOH and −OH groups, while the reduction of Cr(VI) is inhibited after shielding C═O. So, it is reasonable to infer that C═O on the surface of CQDs is the activating functional group to activate PMS.[43]

To further confirm the mechanism of PMS activated by CQDs, the XPS spectra of CQDs before and after reduction reaction were recorded. Figure 7a,b displays the C1s spectrum of CQDs before and after the activation of PMS reaction, respectively. Before the reaction, the XPS spectrum showed a large number of electron-rich functional groups on CQDs, i.e., C═C, C═O, and COOH. After reaction, the size of C═O obviously decreased from 8 to 5%. It can be reasonable to argue that it is consumed in the process of activating PMS. Meanwhile, the oxygen spectra before and after the reaction of the CQD surface were also recorded, as shown in Figure 7c,d. The aforementioned phenomenon, which decreases the size of C═O, can be observed by comparing Figure 7c with Figure 7d. In addition, the same result can be also given from the FT-IR spectra, as shown in Figure S9. The above results authenticate again that the C═O functional group on CQDs plays a major role in activating PMS for Cr(VI) reduction.

The possible activation and reaction mechanism in the CQDs/PMS system is given in Scheme 1. When pH ≤ 2, −OH on the surface of CQDs can directly reduce Cr(VI). When pH ≥ 3, C═O on the surface of CQDs can be employed as an active site to activate PMS and create $O_2^{\bullet-}$ and $^1O_2$ (eqs 5−7).[43,44] The disordered graphitic carbon of CQDs also plays an instrumental role in structural defects and electronic conduction, enabling enhanced catalytic activity.[45] PMS can dissociate H^+, making the solution acidic (pH about 2.6), leading to an increase in the oxidative capacity of Cr(VI). Under this pH condition, the redox potential of Cr(VI) is about 1.1 V, while the redox potentials of $O_2^{\bullet-}$ and $^1O_2$ are about 0.89 and 0.81 V, respectively, as shown in Table S1.[46,47] So, Cr(VI) can oxidize $O_2^{\bullet-}$ and $^1O_2$, leading to its own reduction. The carbonyl group (C═O) on the surface of CQDs is critical in activating PMS to generate $O_2^{\bullet-}$ and $^1O_2$.[48]

$$HSO_5^- + e^- \rightarrow HO_2^\bullet + SO_3^{2-} \quad (5)$$

$$HO_2^\bullet \rightarrow H^+ + O_2^{\bullet-} \quad (6)$$

$$HO_2^\bullet + O_2^{\bullet-} \rightarrow {}^1O_2 \quad (7)$$

5. APPLICATION OF CQDS/PMS IN PRACTICAL WATER SAMPLES

Cl^-, PO_4^{3-}, NO_3^-, and SO_4^{2-} anions usually coexist with Cr(VI) in industrial wastewater and groundwater.[49] The impact of coexisting anions on Cr(VI) reduction by CQDs/PMS was investigated further. As Figure 8a illustrates, the anions (Cl^-, PO_4^{3-}, NO_3^-, and SO_4^{2-}) have no obvious effect on Cr(VI) reduction.

Humic acid (HA) is a yellow-to-black, large-molecule natural organic matter (NOM) that is widely found in water bodies and is commonly considered an organic pollutant. In contrast to the control group without HA addition, adding HA to the solution had virtually no impact on the lowering of Cr(VI) (Figure 8b). A previous study had shown that HA can trap $SO_4^{\bullet-}$ and •OH to influence the reaction rate of catalytic oxidation processes to some extent.[50] It is further shown that $SO_4^{\bullet-}$ and •OH are not the main ROS affecting Cr(VI) reduction.

To replicate the reduction of Cr(VI) in real water samples by CQDs/PMS, 50 mmol/L HA, Cl^-, PO_4^{3-}, NO_3^-, and SO_4^{2-} were added to the Cr(VI) (5 mg/L) solution. As seen in Figure 8c, 99% of Cr(VI) can be reduced within 150 min, and the concentration of Cr(VI) in the solution is only 8 μg/L, which is below the California water quality standard of 10 μg/L.[51]

In addition, cycling experiments (Figure 8d) have shown that CQDs/PMS still has 80% Cr(VI) reduction efficiency after six cycles, showing excellent reuse performance. Similarly, it has been noted in the literature that CQDs can be separated from solution using goethite,[52] for which we tested different concentrations of goethite to separate CQDs, and it can be apparent that when 0.75 g/L goethite is added to the solution (Figure S10), the recovery can reach 82%, indicating that CQDs have good separation performance from solution. The CQDs/PMS system has a higher Cr(VI) reduction efficiency and shorter reduction time than other systems (Table S2).

Similarly, to address the leaching performance of CQDs in aqueous solution, the composite of CQDs and montmorillonite (Mt) was chosen to reduce the secondary pollution of CQDs to the water body, as shown in Figure S11, with obvious CQD particles on Mt. It shows the successful compounding of the materials, and the CQDs/montmorillonite (CMt) composite can be easily filtered out from the water to achieve the effect of convenient recycling. In addition, CMt nanocomposites also exhibit an excellent Cr(VI) reduction and can reduce 94% of Cr(VI) at 120 min (Figure S12). We investigated the CMt cycle experiment and the effect of material recovery further (Figure S13), and it is clear that after three cycles, there are still 41% Cr(VI) reduction efficiency and only 17% mass loss, demonstrating the good recycling performance of CMt.

6. CONCLUSIONS

In summary, CQDs were used to reduce Cr(VI) and explore the reduction mechanism. CQDs can not only directly reduce Cr(VI) at pH 2 but also can activate PMS over a wider pH range to generate ROS for Cr(VI) reduction. At pH 2, Cr(VI) can be reduced by hydroxyl groups on the surface of CQDs. At the same time, the carbonyl group (C═O) on the surface of CQDs can activate PMS to produce specific ROS, i.e., $O_2^{\bullet-}$ and $^1O_2$, to reduce Cr(VI). For simulated wastewater samples containing 5 mg/L Cr(VI), the Cr(VI) concentration can be decreased down below 10 μg/L using the CQDs/PMS system. It provides a new alternative approach to further reducing the toxicity of Cr(VI).

■ ASSOCIATED CONTENT

Supporting Information

The Supporting Information is available free of charge at https://pubs.acs.org/doi/10.1021/acsomega.2c02063.

Methods of making CQD derivatives; reaction diagram of functional groups on the surface of CQDs; FT-IR spectrum of CQDs; UV−vis absorption spectrum and photoluminescence (PL) spectrum of the CQDs; reduction of Cr(VI) by CQDs/PMS at 24 h; FT-IR spectra of CQDs and CQD derivatives; direct reduction

https://doi.org/10.1021/acsomega.2c02063
ACS Omega 2022, 7, 23555−23565

of Cr(VI) by CQDs and their derivatives; FT-IR spectra of CQDs before and after reduction; TEM of Mt and CMt; CMt and CQD activation of PMS for Cr(VI) reduction; redox potential of Cr(VI) and ROS; comparison of Cr(VI) reduction by other materials (PDF)

AUTHOR INFORMATION

Corresponding Author

Guang-Chao Zhao − *School of Ecology and Environment, Anhui Normal University, Wuhu 241000, P. R. China;* orcid.org/0000-0002-7345-6055; Email: gczhao@mail.ahnu.edu.cn

Authors

Wei-Min Yang − *School of Ecology and Environment, Anhui Normal University, Wuhu 241000, P. R. China*

Fu Liu − *School of Ecology and Environment, Anhui Normal University, Wuhu 241000, P. R. China*

Yan-Ting Jin − *School of Ecology and Environment, Anhui Normal University, Wuhu 241000, P. R. China*

Zong-Mu Dong − *School of Ecology and Environment, Anhui Normal University, Wuhu 241000, P. R. China*

Complete contact information is available at: https://pubs.acs.org/10.1021/acsomega.2c02063

Notes

The authors declare no competing financial interest.

ACKNOWLEDGMENTS

The National Nature Science Foundation of China (20975001) and Anhui Normal University collaborated on this project.

REFERENCES

(1) Papaevangelou, V. A.; Gikas, G. D.; Tsihrintzis, V. A. Chromium removal from wastewater using HSF and VF pilot-scale constructed wetlands: Overall performance, and fate and distribution of this element within the wetland environment. *Chemosphere* **2017**, *168*, 716−730.

(2) Ko, Y. J.; Choi, K.; Lee, S.; Jung, K. W.; Hong, S.; Mizuseki, H.; Choi, J. W.; Lee, W. S. Strong chromate-adsorbent based on pyrrolic nitrogen structure: An experimental and theoretical study on the adsorption mechanism. *Water Res.* **2018**, *145*, 287−296.

(3) Bahadır, Z.; Bulut, V. N.; Ozdes, D.; Duran, C.; Bektas, H.; Soylak, M. Separation and preconcentration of lead, chromium and copper by using with the combination coprecipitation-flame atomic absorption spectrometric determination. *J. Ind. Eng. Chem.* **2014**, *20*, 1030−1034.

(4) Li, W.-Q.; Liu, D.; Qu, J.-Y.; Luo, J.-H. Hydrothermal synthesis of a novel nanolayered tin phosphate for removing Cr(iii). *RSC Adv.* **2021**, *11*, 3202−3208.

(5) Wang, N.; Zhu, L.; Deng, K.; She, Y.; Yu, Y.; Tang, H. Visible light photocatalytic reduction of Cr(VI) on TiO_2 in situ modified with small molecular weight organic acids. *Appl. Catal., B* **2010**, *95*, 400−407.

(6) Zhang, Y. C.; Yao, L.; Zhang, G.; Dionysiou, D. D.; Li, J.; Du, X. One-step hydrothermal synthesis of high-performance visible-light-driven SnS_2/SnO_2 nanoheterojunction photocatalyst for the reduction of aqueous Cr(VI). *Appl. Catal., B* **2014**, *144*, 730−738.

(7) Song, L.; Jia, H.; Zhang, H.; Cao, J. Graphene-like h-BN/CdS 2D/3D heterostructure composite as an efficient photocatalyst for rapid removing rhodamine B and Cr(VI) in water. *Ceram. Int.* **2020**, *46*, 24674−24681.

(8) Zuo, Y.; Li, W.; Jiang, L.; Liang, J.; He, G.; Chen, H. ZnCr layered double hydroxide nanoplate-decorated CdS nanowire with excellent photocatalytic activity for removing Cr(VI) in wastewater. *Mater. Lett.* **2020**, *268*, No. 127581.

(9) Li, S.; Wang, C.; Cai, M.; Yang, F.; Liu, Y.; Chen, J.; Zhang, P.; Li, X.; Chen, X. Facile fabrication of $TaON/Bi_2MoO_6$ core−shell S-scheme heterojunction nanofibers for boosting visible-light catalytic levofloxacin degradation and Cr(VI) reduction. *Chem. Eng. J.* **2022**, *428*, No. 131158.

(10) Yu, S.; Tang, H.; Zhang, D.; Wang, S.; Qiu, M.; Song, G.; Fu, D.; Hu, B.; Wang, X. MXenes as emerging nanomaterials in water purification and environmental remediation. *Sci. Total Environ.* **2022**, *811*, No. 152280.

(11) Yu, S.; Pang, H.; Huang, S.; Tang, H.; Wang, S.; Qiu, M.; Chen, Z.; Yang, H.; Song, G.; Fu, D.; Hu, B.; Wang, X. Recent advances in metal-organic framework membranes for water treatment: A review. *Sci. Total Environ.* **2021**, *800*, No. 149662.

(12) Dong, C.; Ji, J.; Shen, B.; Xing, M.; Zhang, J. Enhancement of H_2O_2 Decomposition by the Co-catalytic Effect of WS_2 on the Fenton Reaction for the Synchronous Reduction of Cr(VI) and Remediation of Phenol. *Environ. Sci. Technol.* **A2018**, *52*, 11297−11308.

(13) Li, J.; Wan, Y.; Li, Y.; Yao, G.; Lai, B. Surface Fe(III)/Fe(II) cycle promoted the degradation of atrazine by peroxymonosulfate activation in the presence of hydroxylamine. *Appl. Catal., B* **2019**, *256*, No. 117782.

(14) Li, R.; Dong, H.; Tian, R.; Chen, J.; Xie, Q. Activation of sulfite by different Fe^0-based nanomaterials for oxidative removal of sulfamethazine in aqueous solution. *Sep. Purif. Technol.* **2020**, *250*, No. 117230.

(15) Yin, R.; Guo, W.; Wang, H.; Du, J.; Zhou, X.; Wu, Q.; Zheng, H.; Chang, J.; Ren, N. Enhanced peroxymonosulfate activation for sulfamethazine degradation by ultrasound irradiation: Performances and mechanisms. *Chem. Eng. J.* **2018**, *335*, 145−153.

(16) Lei, Y.; Lu, J.; Zhu, M.; Xie, J.; Peng, S.; Zhu, C. Radical chemistry of diethyl phthalate oxidation via UV/peroxymonosulfate process: Roles of primary and secondary radicals. *Chem. Eng. J.* **2020**, *379*, No. 122339.

(17) Liu, F.; Yang, W.; Li, W.; Zhao, G. C. Simultaneous Oxidation and Sequestration of Arsenic(III) from Aqueous Solution by Copper Aluminate with Peroxymonosulfate: A Fast and Efficient Heterogeneous Process. *ACS Omega* **2021**, *6*, 1477−1487.

(18) Zhang, Y.; Xu, X.; Cao, L.; Ok, Y. S.; Cao, X. Characterization and quantification of electron donating capacity and its structure dependence in biochar derived from three waste biomasses. *Chemosphere* **2018**, *211*, 1073−1081.

(19) Qiu, M.; Liu, L.; Ling, Q.; Cai, Y.; Yu, S.; Wang, S.; Fu, D.; Hu, B.; Wang, X. Biochar for the removal of contaminants from soil and water: a review. *Biochar* **2022**, *4*, 19.

(20) Baker, S. N.; Baker, G. A. Luminescent carbon nanodots: emergent nanolights. *Angew Chem., Int Ed.* **2010**, *49*, 6726−6744.

(21) Tian, L.; Li, Z.; Wang, P.; Zhai, X.; Wang, X.; Li, T. Carbon quantum dots for advanced electrocatalysis. *J. Energy Chem.* **2021**, *55*, 279−294.

(22) Guo, Y.; Wang, Z.; Shao, H.; Jiang, X. Hydrothermal synthesis of highly fluorescent carbon nanoparticles from sodium citrate and their use for the detection of mercury ions. *Carbon* **2013**, *52*, 583−589.

(23) Sun, D.; Liu, T.; Wang, C.; Yang, L.; Yang, S.; Zhuo, K. Hydrothermal synthesis of fluorescent carbon dots from gardenia fruit for sensitive on-off-on detection of Hg(2+) and cysteine. *Spectrochim. Acta, Part A* **2020**, *240*, No. 118598.

(24) Zhu, S.; Meng, Q.; Wang, L.; Zhang, J.; Song, Y.; Jin, H.; Zhang, K.; Sun, H.; Wang, H.; Yang, B. Highly photoluminescent carbon dots for multicolor patterning, sensors, and bioimaging. *Angew Chem., Int. Ed.* **2013**, *52*, 3953−3957.

(25) Zhao, Q.-L.; Zhang, Z.-L.; Huang, B.-H.; Peng, J.; Zhang, M.; Pang, D.-W. Facile preparation of low cytotoxicity fluorescent carbon nanocrystals by electrooxidation of graphite. *Chem. Commun.* **2008**, *41*, 5116−5118.

(26) Gu, H.; Rapole, S. B.; Huang, Y.; Cao, D.; Luo, Z.; Wei, S.; Guo, Z. Synergistic interactions between multi-walled carbon nanotubes and toxic hexavalent chromium. *J. Mater. Chem. A* **2013**, *1*, 2011−2021.

(27) Li, H.; Li, N.; Zuo, P.; Qu, S.; Shen, W. Efficient adsorption-reduction synergistic effects of sulfur, nitrogen and oxygen heteroatom

co-doped porous carbon spheres for chromium(VI) removal. *Colloids Surf., A* **2021**, *618*, No. 126502.
(28) Sun, Y.; Yue, Q.; Gao, B.; Gao, Y.; Li, Q.; Wang, Y. Adsorption of hexavalent chromium on Arundo donax Linn activated carbon amine-crosslinked copolymer. *Chem. Eng. J.* **2013**, *217*, 240−247.
(29) Liu, L.; Liu, X.; Wang, D.; Lin, H.; Huang, L Removal and reduction of Cr(VI) in simulated wastewater using magnetic biochar prepared by co-pyrolysis of nano-zero-valent iron and sewage sludge. *J. Cleaner Prod.* 2020, *257*, 120562, DOI: 10.1016/j.jclepro.2020.120562
(30) Kotaś, J.; Stasicka, Z. Chromium occurrence in the environment and methods of its speciation. *Environ. Pollut.* **2000**, *107*, 263−283.
(31) Mohamed, A.; Osman, T. A.; Toprak, M. S.; Muhammed, M.; Yilmaz, E.; Uheida, A. Visible light photocatalytic reduction of Cr(VI) by surface modified CNT/titanium dioxide composites nanofibers. *J. Mol. Catal. A-Chem.* **2016**, *424*, 45−53.
(32) Chen, H.; Zhang, Z.; Zhong, X.; Zhuo, Z.; Tian, S.; Fu, S.; Chen, Y.; Liu, Y. Constructing MoS_2/Lignin-derived carbon nanocomposites for highly efficient removal of Cr(VI) from aqueous environment. *J. Hazard. Mater.* **2021**, *408*, No. 124847.
(33) Golshan, M.; Kakavandi, B.; Ahmadi, M.; Azizi, M. Photocatalytic activation of peroxymonosulfate by TiO_2 anchored on cupper ferrite (TiO_2@$CuFe_2O_4$) into 2,4-D degradation: Process feasibility, mechanism and pathway. *J. Hazard. Mater.* **2018**, *359*, 325−337.
(34) Li, X.; Liu, X.; Huang, X.; Lin, C.; He, M.; Ouyang, W. Activation of peroxymonosulfate by WTRs-based iron-carbon composites for atrazine removal: Performance evaluation, mechanism insight and byproduct analysis. *Chem. Eng. J.* **2021**, *421*, No. 127811.
(35) Han, W.; Li, D.; Zhang, M.; Ximin, H.; Duan, X.; Liu, S.; Wang, S. Photocatalytic activation of peroxymonosulfate by surface-tailored carbon quantum dots. *J. Hazard. Mater.* **2020**, *395*, No. 122695.
(36) Lee, H.; Kim, H. I.; Weon, S.; Choi, W.; Hwang, Y. S.; Seo, J.; Lee, C.; Kim, J. H. Activation of Persulfates by Graphitized Nanodiamonds for Removal of Organic Compounds. *Environ. Sci. Technol.* **2016**, *50*, 10134−10142.
(37) Lee, J.; Mackeyev, Y.; Cho, M.; Li, D.; Kim, J.-H.; Wilson, L. J.; Alvarez, P. J. Photochemical and Antimicrobial Properties of Novel C_{60} Derivatives in Aqueous Systems. *Environ. Sci. Technol.* **2009**, *43*, 6604−6610.
(38) Zhang, H.; Xiao, R.; Li, R.; Ali, A.; Chen, A.; Zhang, Z. Enhanced aqueous Cr(VI) removal using chitosan-modified magnetic biochars derived from bamboo residues. *Chemosphere* **2020**, *261*, No. 127694.
(39) Wang, Y.; Hu, A. Carbon quantum dots: synthesis, properties and applications. *J. Mater. Chem. C* 2014, *2*(), 6921-6939, DOI: 10.1039/C4TC00988F.
(40) Cheng, X.; Guo, H.; Zhang, Y.; Korshin, G. V.; Yang, B. Insights into the mechanism of nonradical reactions of persulfate activated by carbon nanotubes: Activation performance and structure-function relationship. *Water Res.* **2019**, *157*, 406−414.
(41) Chen, Y.; An, D.; Sun, S.; Gao, J.; Qian, L. Reduction and Removal of Chromium VI in Water by Powdered Activated Carbon. *Materials* 2018, *11*(), 269, DOI: 10.3390/ma11020269.
(42) Yao, Y.; Zhang, J.; Chen, H.; Yu, M.; Gao, M.; Hu, Y.; Wang, S. Ni^0 encapsulated in N-doped carbon nanotubes for catalytic reduction of highly toxic hexavalent chromium. *Appl. Surf. Sci.* **2018**, *440*, 421−431.
(43) Li, J.; Li, M.; Sun, H.; Ao, Z.; Wang, S.; Liu, S. Understanding of the Oxidation Behavior of Benzyl Alcohol by Peroxymonosulfate via Carbon Nanotubes Activation. *ACS Catal.* **2020**, *10*, 3516−3525.
(44) Wang, J.; Wang, S. Reactive species in advanced oxidation processes: Formation, identification and reaction mechanism. *Chem. Eng. J.* **2020**, *401*, No. 126158.
(45) Sun, Q.; Yu, Z.; Jiang, R.; Hou, Y.; Sun, L.; Qian, L.; Li, F.; Li, M.; Ran, Q.; Zhang, H. CoP QD anchored carbon skeleton modified CdS nanorods as a co-catalyst for photocatalytic hydrogen production. *Nanoscale* **2020**, *12*, 19203−19212.
(46) Jawad, A.; Zhan, K.; Wang, H.; Shahzad, A.; Zeng, Z.; Wang, J.; Zhou, X.; Ullah, H.; Chen, Z.; Chen, Z. Tuning of Persulfate Activation from a Free Radical to a Nonradical Pathway through the Incorporation of Non-Redox Magnesium Oxide. *Environ. Sci. Technol.* **2020**, *54*, 2476−2488.
(47) Zhu, S.; Li, X.; Kang, J.; Duan, X.; Wang, S. Persulfate Activation on Crystallographic Manganese Oxides: Mechanism of Singlet Oxygen Evolution for Nonradical Selective Degradation of Aqueous Contaminants. *Environ. Sci. Technol.* **2019**, *53*, 307−315.
(48) Li, D.; Duan, X.; Sun, H.; Kang, J.; Zhang, H.; Tade, M. O.; Wang, S. Facile synthesis of nitrogen-doped graphene via low-temperature pyrolysis: The effects of precursors and annealing ambience on metal-free catalytic oxidation. *Carbon* **2017**, *115*, 649−658.
(49) Jia, J.; Liu, D.; Tian, J.; Wang, W.; Ni, J.; Wang, X. Visible-light-excited humic acid for peroxymonosulfate activation to degrade bisphenol A. *Chem. Eng. J.* **2020**, *400*, No. 125853.
(50) Sharma, J.; Mishra, I. M.; Dionysiou, D. D.; Kumar, V. Oxidative removal of Bisphenol A by UV-C/peroxymonosulfate (PMS): Kinetics, influence of co-existing chemicals and degradation pathway. *Chem. Eng. J.* **2015**, *276*, 193−204.
(51) Pan, C.; Troyer, L. D.; Catalano, J. G.; Giammar, D. E. Dynamics of Chromium(VI) Removal from Drinking Water by Iron Electrocoagulation. *Environ. Sci. Technol.* **2016**, *50*, 13502−13510.
(52) Liu, X.; Li, J.; Huang, Y.; Wang, X.; Zhang, X.; Wang, X. Adsorption, Aggregation, and Deposition Behaviors of Carbon Dots on Minerals. *Environ. Sci. Technol.* **2017**, *51*, 6156−6164.

https://doi.org/10.1021/acsomega.2c02063
ACS Omega 2022, 7, 23555−23565